Full-field FRF estimation from noisy high-speed-camera data using a dynamic substructuring approach

Tomaž Bregar[a], Klemen Zaletelj[b], Gregor Čepon[b,*], Janko Slavič[b], Miha Boltežar[b]

[a] *Gorenje d.o.o., Partizanska 12, 3503 Velenje, Slovenia*
[b] *University of Ljubljana, Faculty of Mechanical Engineering, Aškerčeva 6, 1000 Ljubljana, Slovenia*

Cite as:
Tomaž Bregar, Klemen Zaletelj, Gregor Čepon, Janko Slavič, Miha Boltežar, Full-field FRF estimation from noisy high-speed-camera data using a dynamic substructuring approach, Mechanical Systems and Signal Processin 2020, https://doi.org/10.1016/j.ymssp.2020.107263

Abstract

The use of a high-speed camera for dynamic measurements is becoming a compelling alternative to accelerometers and laser vibrometers. However, the estimated displacements from a high-speed camera generally exhibit relatively high levels of noise. This noise has proven to be problematic in the high-frequency range, where the amplitudes of the displacements are typically very small. Nevertheless, the mode shapes of the structure can be identified even in the frequency range where the noise is dominant, by using eigenvalues from a Least-Squares Complex Frequency identification on accelerometer measurements. The identified mode shapes from the Least-Squares Frequency-Domain method can then be used to estimate the full-field FRFs. However, the reconstruction of the FRFs from the identified modeshapes is not consistent in the high-frequency range. In this paper a novel methodology is proposed for an improved experimental estimation of full-field FRFs using a dynamic substructuring approach. The recently introduced System Equivalent Model Mixing is used to form a hybrid model from two different experimental models of the same system. The first model is the reconstructed full-field FRFs that contribute the full-field DoF set and the second model is the accelerometer measurements that provide accurate dynamic characteristics. Therefore, no numerical or analytical model is required for the expansion. The experimental case study demonstrates the increased accuracy of the estimated FRFs of the hybrid model, especially in the high-frequency range, when compared to existing methods.

Keywords: hybrid model, frequency-based substructuring, system equivalent model mixing, high-speed camera, full-field FRFs

*Corresponding author
Email address: gregor.cepon@fs.uni-lj.si (Gregor Čepon)

1 Introduction

Displacement identification based on high-speed-camera measurements has become more popular in recent years compared to traditional measurement methods [1, 2]. Although accurate, acceleration transducers allow the user to acquire the dynamic information only at discrete points and even a relatively small mass of the accelerometer can impose a problem, especially with lightweight structures [3]. Non-contact methods, such as laser vibrometry, can be used to measure the dynamic response of the structure at discrete locations [4]. Scanning laser vibrometer systems can be used to scan the entire surface; however, the measurements are not instantaneous and only the response in one direction can be obtained [5].

Optical measurements offer a spatially dense measurement, as each image pixel can be used as a measurement location. With clear advantages of optical measurements, camera-based systems were used for modal parameter identification [6, 7], for dynamic strain measurements [8, 9] and for applications in the automotive industry [10], aerospace industry [11] and in civil engineering [12, 13]. Different methods can be used to identify the displacements from consecutive images. Generally, Digital Image Correlation (DIC) [14, 15], Gradient-Based Optical Flow (GBOF) [16, 17] and Phase-Based methods [18, 19] are used for displacement identification. Even with distinct differences between each identification methodology, all of them share the same disadvantage. The limitation that the noise floor associated with the camera and the identification method used is the same or even larger than the measured displacement response [20]. The absolute value of the response is highly case-specific; however, for lab-scale structures the amplitude of displacements above 1 kHz is usually relatively small, typically less than several micrometers [16].

Advanced modal identification methods such as the Least-Squares Complex Frequency (LSCF) [21] in combination with the Least-Squares Frequency Domain (LSFD) [22] can be used to determine the modal parameters even on relatively noisy and inconsistent data sets [23]. However, the displacements identified with a high-speed camera can introduce a problem for these modal identification methods, since the vibration response is often masked by the camera's noise floor. A combined accelerometer/camera mode-shape identification was introduced [24], where both acceleration and displacement data are used. The method has shown an improvement in the overall frequency range that can be utilized in the modal identification as the mode shapes can be identified at a displacement resolution up to 1/100000 of a pixel [24]. However, the reconstruction of FRFs from the identified mode shapes is not accurate in the high-frequency range where the noise is predominant. An inconsistency in the real and imaginary parts of the full-field FRFs can be observed when compared with the reference measurements [24].

The objective of this paper is to improve the accuracy of full-field FRFs from a high-speed camera, especially in the high-frequency range where the noise is predominant. Therefore, the novel methodology presented in this paper proposes a hybrid approach to incorporate strong suits of full-field noisy measurements from a high-speed camera with accurate measurements from an accelerometer into a single model. This is referred to as the mixing of multiple equivalent experimental models of the same component into a hybrid model using dynamic substructuring techniques [25, 26, 27]. It represents a hybrid and therefore very powerful modeling approach that would not follow an updating scheme which could remove the physically relevant information of the system [28]. The hybrid model is established using the recently developed System Equivalent Model Mixing (SEMM) method [26]. With SEMM different dynamic models of the same system can be mixed into one hybrid model based on the Lagrange Multiplier Frequency-Based Substructuring (LM FBS) method [29]. SEMM could also be regarded as an expansion method, where the experimental model is projected onto an unmeasured DoF set [30]. Finally, an experimental case study demonstrates the efficiency and accuracy of the proposed approach. The quality of the reconstructed FRFs was evaluated in comparison with a reference measurement using a coherence criterion. The hybrid modeling approach demonstrates the significantly higher coherence values of the reconstructed full-field FRFs in the high-frequency range compared to existing methods.

The paper is organized as follows. The next section summarizes the basic theory behind the modal identification of optical flow data, followed by an overview of the system-equivalent-mixing methodology and Lagrange multiplier frequency-based substructuring. In Section 3 a novel methodology for obtaining hybrid full-field FRFs from high-speed-camera data is introduced. In Section 4 an experimental validation of the methodology is performed on a lab-scale experiment. Finally, the conclusions are drawn in Section 5.

2 Theoretical background

2.1 Modal parameter identification of optical flow data

High-speed-camera-based measurements produce a sequence of images that carry information about the motion of objects. Each pixel has an intensity value that changes over time, as the object changes its position on the image. Simplified Gradient-Based Optical Flow (SGBOF) [16] can be used for the displacement identification on each separate image pixel. If the local intensity gradient is assumed to be constant, a linear relation between the change in pixel intensity ΔI and object displacement Δs can be obtained as follows:

$$\Delta s(x,y,t) = \frac{I(x,y,t) - I(x,y,t+\Delta t)}{|\nabla I_0|} \pm \sqrt{\Delta x_L^2 + \Delta y_L^2}, \tag{1}$$

where Δx_L^2 and Δy_L^2 are the integer displacements used when the object's motion exceeds half of a pixel in the x or y direction. $|\nabla I_0|$ is the scalar value of the intensity gradient and I_0 is the intensity gradient of the reference image. Since Δs represents the absolute displacements, the direction correction needs to be used if the directional displacements are required:

$$\Delta x(x,y,t) = \frac{\frac{\partial I}{\partial x}}{|\nabla I_0|}\,\Delta s(x,y,t). \tag{2}$$

A high-intensity gradient is needed for a consistent displacement identification, since the sensitivity of the SGBOF increases with the intensity gradient (see Eq. (1)). A speckle pattern or a similar pattern design is used on the measured surface to increase the intensity gradient. With a single high-speed camera in one set-up only 2D displacements can be measured; however, if a stereoscopic set-up is used, also 3D measurements can be performed [31]. Recently, frequency-domain triangulation was introduced for 3D operating-deflection-shape identification [32].

Even with a proper pattern the measured data is generally relatively noisy. The noise imposes a problem on modal identification, especially in the frequency range where the amplitude of the measured response is close to the overall noise level. The use of advanced modal identification techniques on the identified displacements with the SGBOF, such as the Least-Squares Complex Frequency (LSCF) method [21], are commonly inconsistent, or the modal parameters cannot even be identified. However, this problem can be resolved by using a combined accelerometer/camera identification [24]. First, from the accelerometer measurements the system's complex eigenvalues ${}_{acc}\lambda_r$ are obtained, which contain the eigenfrequencies ω_r and the damping ratios ζ_r:

$${}_{acc}\lambda_r = -\zeta_r\,\omega_r \pm \mathrm{i}\,\omega_r\,\sqrt{1-\zeta_r^2}. \tag{3}$$

The identified ${}_{acc}\lambda_r$ are then applied to the Least-Squares Frequency Domain (LSFD) method [33] to determine the modal constants ${}_rA_j$ together with the upper and lower residuals A_U and A_L:

$${}_{cam}Y_j(\omega) = \sum_{r=1}^{N}\left(\frac{{}_rA_j}{\mathrm{i}\,\omega - {}_{acc}\lambda_r} + \frac{{}_rA_j^*}{\mathrm{i}\,\omega - {}_{acc}\lambda_r^*}\right) - \frac{A_L}{\omega^2} + A_U, \tag{4}$$

where * denotes a complex conjugate and the subscript j the location of each separate pixel. For each location, all the frequency points are taken into account to construct an over-determined set of equations from Eq. (4). Each equation set is then solved for the modal constants, upper and lower residuals using the least-squares method.

2.2 System equivalent model mixing

System Equivalent Model Mixing (SEMM) [26] makes it possible to mix multiple equivalent-response models of the same system using Lagrange Multiplier Frequency-Based Substructuring (LM FBS) [29]. A schematic representation of SEMM is shown in Fig. 12. One of the models provides the dynamic properties (overlay model) and the second model provides a full DoF set (parent model). The dynamic properties of the parent model are, at the end, removed (removed model) from the final model (hybrid model).

Before introducing the basic theory of SEMM, a short recap of LM FBS [29] is provided. The LM FBS is primarily used to determine the admittance of an

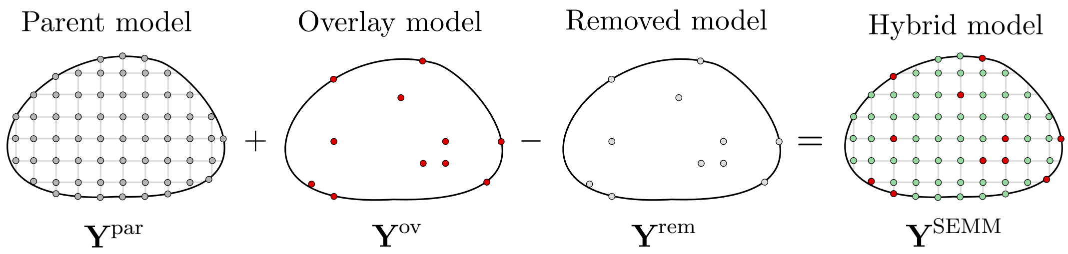

Figure 1: Schematic representation of System Equivalent Model Mixing.

assembled system $\mathbf{Y}^{\text{AB}}$ by coupling the admittances of two separate substructures $\mathbf{Y}^{\text{A}}$ and $\mathbf{Y}^{\text{B}}$. The equation of motion of the uncoupled system can be written in a block-diagonal form as:[1]

$$\mathbf{u} = \mathbf{Y}(\mathbf{f}+\mathbf{g}); \text{ where } \mathbf{Y}^{\text{A|B}} = \begin{bmatrix} \mathbf{Y}^{\text{A}} & \mathbf{0} \\ \mathbf{0} & \mathbf{Y}^{\text{B}} \end{bmatrix}, \mathbf{u} = \begin{bmatrix} \mathbf{u}^{\text{A}} \\ \mathbf{u}^{\text{B}} \end{bmatrix}, \mathbf{f} = \begin{bmatrix} \mathbf{f}^{\text{A}} \\ \mathbf{f}^{\text{B}} \end{bmatrix}, \mathbf{g} = \begin{bmatrix} \mathbf{g}^{\text{A}} \\ \mathbf{g}^{\text{B}} \end{bmatrix}, \tag{5}$$

where $\mathbf{u}$ denotes the vector of displacements, $\mathbf{f}$ the vector of external forces and $\mathbf{g}$ the vector of interface forces. The substructures can be coupled by defining two sets of constraints. These are the compatibility and equilibrium conditions, which can be defined in matrix notation by a signed Boolean matrix:

$$\text{Compatibility:} \quad \mathbf{B}\mathbf{u} = \mathbf{0}; \qquad \text{Equilibrium:} \quad \mathbf{g} = -\mathbf{B}^{\text{T}}\boldsymbol{\lambda}, \tag{6}$$

where $\boldsymbol{\lambda}$ denotes the unknown Lagrange multipliers representing the reaction forces between the two substructures. Inserting the conditions of compatibility and equilibrium Eq. (6) into Eq. (5) and eliminating $\boldsymbol{\lambda}$ yields the admittance matrix of the assembled system [29]:

$$\mathbf{Y}^{\text{AB}}\mathbf{f} = \left(\mathbf{Y}^{\text{A|B}} - \mathbf{Y}^{\text{A|B}}\mathbf{B}^{\text{T}}(\mathbf{B}\mathbf{Y}^{\text{A|B}}\mathbf{B}^{\text{T}})^{-1}\mathbf{B}\mathbf{Y}^{\text{A|B}}\right)\mathbf{f}. \tag{7}$$

With the SEMM the LM FBS methodology is used to calculate a hybrid model by coupling the dynamic properties of two separate models of the same component on their shared DoF. The hybrid model is generally formed by mixing a numerical with an experimental model. A numerical model is commonly used as a parent model, which provides the full DoF set and an experimental model is used as an overlay model, which provides the dynamic properties. The equation of motion for the uncoupled model can be formulated as follows:

$$\mathbf{u} = \mathbf{Y}(\mathbf{f}+\mathbf{g}); \text{ where } \mathbf{Y} = \begin{bmatrix} \mathbf{Y}^{\text{par}} & \mathbf{0} & \mathbf{0} \\ \mathbf{0} & -\mathbf{Y}^{\text{rem}} & \mathbf{0} \\ \mathbf{0} & \mathbf{0} & \mathbf{Y}^{\text{ov}} \end{bmatrix}, \mathbf{f} = \begin{bmatrix} \mathbf{f}^{\text{par}} \\ \mathbf{f}^{\text{rem}} \\ \mathbf{f}^{\text{ov}} \end{bmatrix}, \mathbf{g} = \begin{bmatrix} \mathbf{g}^{\text{par}} \\ \mathbf{g}^{\text{rem}} \\ \mathbf{g}^{\text{ov}} \end{bmatrix} \tag{8}$$

[1]An explicit dependency on the frequency is omitted in order to simplify the notation, and also in the remainder of the paper.

where $\mathbf{Y}^{\mathrm{par}}$ denotes the admittance FRF matrix of the parent model (numerical model), $\mathbf{Y}^{\mathrm{rem}}$ the removed model and $\mathbf{Y}^{\mathrm{ov}}$ the overlay model (experimental model). Vector $\mathbf{f}$ represents the applied forces to the system and vector $\mathbf{g}$ the interface forces of each model. Note that the admittance of the removed model is negative to decouple the dynamics of the parent model.

The parent model can only be decoupled as a whole or as a reduced model at the overlay DoF. However, if the dynamics of the parent model are decoupled only at the overlay DoF, spurious peaks can occur in the hybrid model [26]. This is due to the condensed removed interface $\mathbf{Y}^{\mathrm{rem}}$, as not all the dynamic properties of the parent model are removed in the decoupling step. The problem with the conflicting dynamics can be resolved by expanding the size of the removed interface and decoupling the dynamics of the parent model as a whole ($\mathbf{Y}^{\mathrm{rem}} = \mathbf{Y}^{\mathrm{par}}$). In this paper the expanded interface is used for the derivation.

To couple or uncouple the different models using the LM FBS [29] the two conditions must be satisfied at the interface. The first is the condition of compatibility:

$$\mathbf{u}_g^{\mathrm{par}} - \mathbf{u}_g^{\mathrm{rem}} = \mathbf{0}; \quad \mathbf{u}_i^{\mathrm{rem}} - \mathbf{u}_i^{\mathrm{ov}} = \mathbf{0}, \tag{9}$$

where the subscript g denotes the global DoF set combining the boundary and the internal DoF set, which are denoted with a subscript i. These are the shared DoFs between the overlay and the parent model. The second condition is the force equilibrium:

$$\mathbf{g}_b^{\mathrm{par}} + \mathbf{g}_b^{\mathrm{rem}} = \mathbf{0}; \quad \mathbf{g}_i^{\mathrm{par}} + \mathbf{g}_i^{\mathrm{rem}} + \mathbf{g}_i^{\mathrm{ov}} = \mathbf{0} \tag{10}$$

where the subscript b denotes the boundary DoF set. Both conditions can be written in matrix notation using a signed Boolean matrix $\mathbf{B}$ and a set of Lagrange multipliers $\boldsymbol{\lambda}$ as follows:

$$\mathbf{B}\mathbf{u} = \mathbf{0}, \quad \mathbf{g} = -\mathbf{B}^{\mathrm{T}}\boldsymbol{\lambda}; \quad \text{where} \quad \mathbf{B} = \left[\begin{array}{cc|cc|c} \mathbf{I} & \mathbf{0} & -\mathbf{I} & \mathbf{0} & \mathbf{0} \\ \mathbf{0} & \mathbf{I} & \mathbf{0} & -\mathbf{I} & \mathbf{0} \\ \mathbf{0} & \mathbf{0} & \mathbf{I} & \mathbf{0} & -\mathbf{I} \end{array}\right]. \tag{11}$$

The equations can be solved using the LM FBS method [29]. Reformulating it as a primal notation, which results in a single-line formulation for the hybrid SEMM model [26]:

$$\mathbf{Y}^{\mathrm{SEMM}} = \mathbf{Y}_{gg} - \mathbf{Y}_{gg}^{\mathrm{par}}\big(\mathbf{Y}_{bg}^{\mathrm{rem}}\big)^{+}\big(\mathbf{Y}_{bb}^{\mathrm{rem}} - \mathbf{Y}_{bb}^{\mathrm{ov}}\big)\big(\mathbf{Y}_{gb}^{\mathrm{rem}}\big)^{+}\mathbf{Y}_{gg}^{\mathrm{par}}. \tag{12}$$

The SEMM can also be regarded as an expansion technique where a limited experimental DoF set (overlay model) is projected onto the larger numerical DoF set (parent model). One of the primary advantages of the SEMM is, even though a DoF set is expanded, the final hybrid model remains a full-rank model. This is the main difference between the SEMM and other popular expansion techniques, such as the physical expansion methods [34, 35] or modal expansion [36, 37, 38] techniques, where the full-rank model is lost in the condensation process [30].

The use of the SEMM to mix numerical and experimental models was already demonstrated on simple lab-scale structures. Moreover, the use of the SEMM has already proven to be advantageous on more complex structures, for instance, the methodology was already used on an automotive subcomponent [39].

3 Increasing the consistency of identified full-field FRFs using SEMM

Here, a methodology is proposed to reduce the inconsistency of identified full-field FRFs by using the System Equivalent Model Mixing methodology. For the combined accelerometer/camera mode-shape identification two different response models are already used [24]. The first one consists of the identified full-field displacements from the high-speed camera and the second model is the accurate accelerometer measurements. With the current approach the mode shapes can be identified, even in the frequency range where the noise is predominant. However, when the reconstructed FRFs are compared with a reference, an inconsistency in the real and imaginary parts of the FRF can be observed [24].

The inconsistency can be resolved with an additional computational step in the identification procedure, where the SEMM is used. The response model from the accelerometer measurements is used as an overlay model to correct the reconstructed full-field FRFs from a high-speed camera (used as the parent model):

$$\mathbf{Y} = \begin{bmatrix} \mathbf{Y}_{\mathrm{cam}}^{\mathrm{par}} & \mathbf{0} & \mathbf{0} \\ \mathbf{0} & -\mathbf{Y}^{\mathrm{rem}} & \mathbf{0} \\ \mathbf{0} & \mathbf{0} & \mathbf{Y}_{\mathrm{acc}}^{\mathrm{ov}} \end{bmatrix}. \tag{13}$$

A schematic depiction of the whole hybrid-identification approach for the full-field FRFs estimation is shown in Fig. 2. First, the displacement is identified from the high-speed-camera measurements (Eq. (2)). Simultaneously, an accurate response model from the accelerometer measurements can be obtained. In the next step the mode shapes are estimated based on the combined accelerometer/camera identification [24]. Finally, the reconstructed FRFs from the estimated mode shapes are used as a parent model and the accelerometer measurements are used as the overlay model in the SEMM (Eq. (12)).

The SEMM is generally used to mix a numerical model (the parent model provides the DoF set) with an experimental model (the overlay model provides the dynamic properties). Therefore, a full-response model for the parent model is always accessible from the numerical model.[2] Due to the use of an experimental model as the parent model, the full-response model cannot be obtained in practise.

The reduced size of the parent model and with that also the reduced size of the removed model imposes certain limitations on the decoupling step in the SEMM. If a full-response model is used for the parent model and subsequently also for the removed model, the hybrid model on the interface DoF only includes the dynamic

[2]When referring to a full-response model a full-FRF admittance matrix is considered. The FRFs for each response DoF are determined for the excitation at each separate DoF; therefore, the admittance matrix for each frequency line is in fact a square matrix.

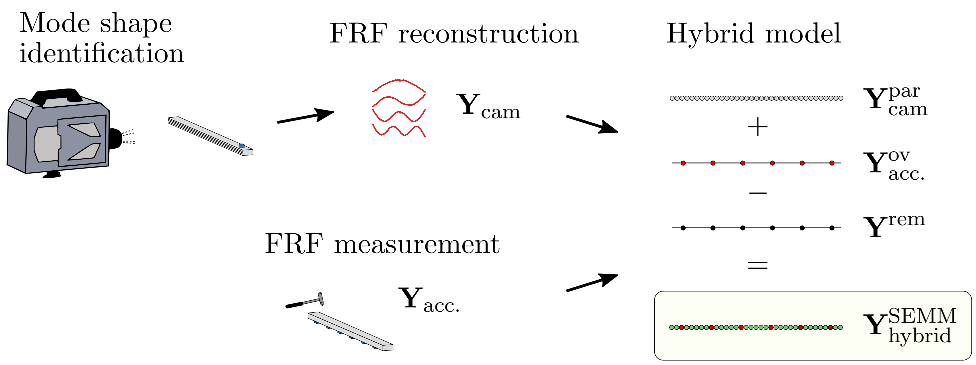

Figure 2: Schematic depiction of the identification of full-field hybrid FRFs from high-speed-camera measurements using the SEMM.

properties of the overlay model (the dynamic properties of the parent model are removed completely). That is not the case with the use of a reduced parent model, where at the interface DoF the dynamic properties of the parent model will still be present, even after the decoupling step. The reason is due to the relatively poor observability and controllability of the reduced interface. If the leftover parent dynamics were to impose a problem, an objective criterion, such as the Interface Completeness Criterion (ICC), should be used to evaluate the quality of the decoupling step [40]. Furthermore, the DoFs used at the interface in SEMM, overlapping between the parent and the overlay model, have to be collocated. As both the parent and the overlay model are experimental models in the proposed methodology, care should be taken, not to introduce unwanted bias between the two models. Additionally, in the hybrid full-field FRFs estimation only the identified DoFs from the high-speed camera are available.

The proposed hybrid estimation of the full-field FRFs can be summarized as follows:

1. Displacement identification from high-speed-camera measurements (Eq. (2)).
2. Combined accelerometer/camera mode-shape estimation from system complex eigenvalues identified from accelerometer data (Sec. 2.1).
3. Reconstruction of the full-field FRFs based on the identified mode shapes (Eq. (4)).
4. Calculation of a hybrid model from the reconstructed FRFs with the accelerometer measurements using the SEMM.

4 Experiment

An experiment was performed on a solid steel beam with dimensions $12 \times 40 \times 600$ mm. The beam was supported on polyurethane-foam blocks representing approximately free-free boundary conditions. The experimental setup is shown in Figure 3. Two different experimental models were acquired. The first one from six equally spaced accelerometers and the second one from the high-speed camera. An additional accelerometer was used as a reference, where the proposed methodology was validated.

Dytran 3097A2T uni-axial accelerometers weighing 4.3 g were used to measure the response and a PCB 086C03 modal hammer with a hard metal tip was used to excite the structure. A Fastcam SA-Z high-speed camera was used to measure the response. A pattern with horizontal lines was added to the front face of the beam in order to maximize the pixel intensity gradient in the vertical direction. The camera was set to have a resolution of 1024×48 pixels and was recording at 200000 frames per second. The displacements were identified at 1000 points along the length of the beam with the SGBOF (Eq. (2)).

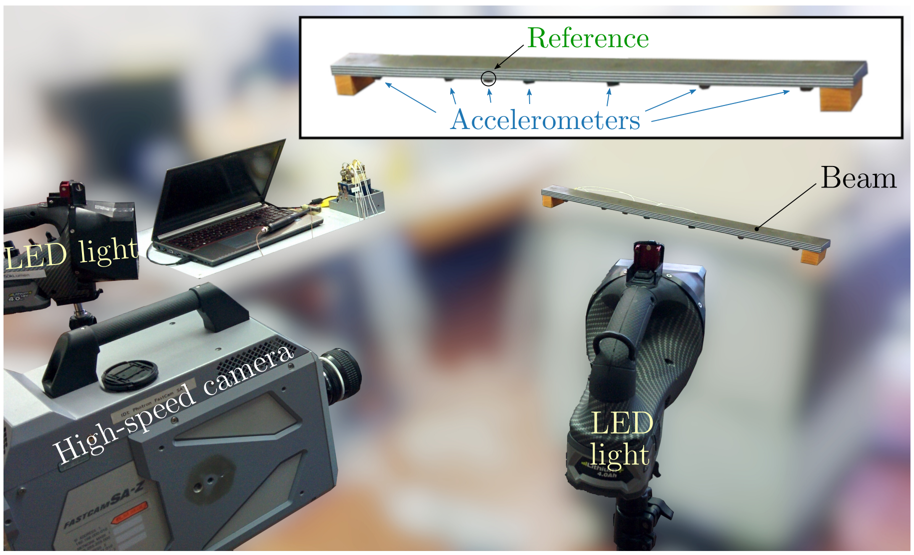

Figure 3: Photograph of the experimental setup with the high-speed camera.

4.1 Identification of the mode shapes

A combined accelerometer/camera mode-shape identification [24] was used to identify the mode shapes of the steel beam. System complex eigenvalues from the accelerometer model were determined from a stabilization diagram using the LSCF. Accelerometer eigenvalues were then used in the LSFD identification (see Eq. (4)) and altogether eight mode shapes were determined in the frequency range up to 6 kHz. All the identified mode shapes are shown in Fig. 4. The advantage of a full-field identification of the mode shapes can be clearly seen in the increased spatial resolution.

The limitations of discrete measurements using accelerometers are observable also from the AutoMAC[3] criterion depicted in Fig. 5. Up to the 4th mode shape

[3]Modal Assurance Criterion (MAC) [39] is defined as a scalar constant relating to the degree of consistency (linearity) between two mode shapes. The AutoMAC compares a set of mode shapes to itself using a MAC criterion.

the spatial resolution with the discrete accelerometers measurements is sufficient to identify the corresponding mode shapes. However, in the high frequency range, the spatial resolution of accelerometer is not adequate to deduce the corresponding mode shapes. This can be interpreted as a spatial aliasing and consequently the real mode shape cannot be identified. Similar observation can be made when comparing mode shapes from the accelerometer and the high-speed camera using the MAC criterion (see Fig. 5).

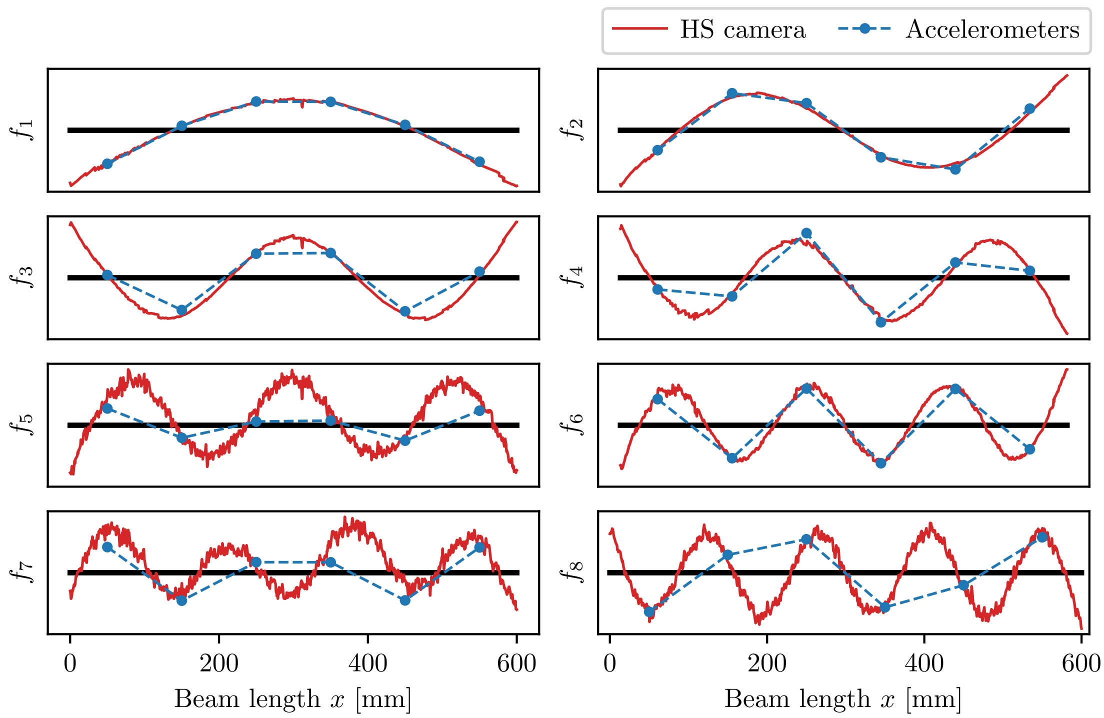

Figure 4: Identified mode shapes from high-speed camera and accelerometers using the LSCF/LSFD identification.

4.2 Hybrid model from accelerometer and high-speed-camera data

In the final step a hybrid model is formed from the high-speed-camera and accelerometer measurements. With the proposed methodology an experimental model is used as the parent model; therefore, a full-response model for the parent model is not available. In the current configuration one would need to measure at 1000 different impact locations to acquire the full-response model. That is not achievable in practise, and for this reason a smaller response model was used for the construction of the hybrid model. In this research only one impact location was used. The dimensions of each separate model are therefore equal to:

$$\mathbf{Y}_{\text{cam}}^{\text{par}} \in \mathbb{C}^{1000\times1}, \quad \mathbf{Y}_{\text{acc}}^{\text{ov}} \in \mathbb{C}^{6\times1}, \quad \mathbf{Y}_{\text{hybrid}}^{\text{SEMM}} \in \mathbb{C}^{1000\times1}. \tag{14}$$

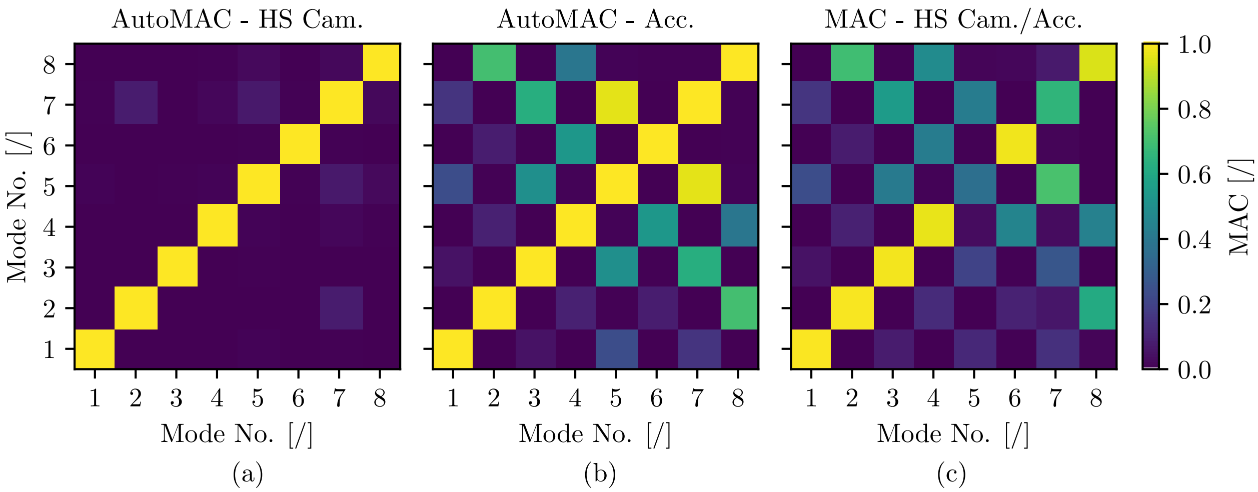

Figure 5: Comparison of identified mode shapes from high-speed camera and accelerometers using an AutoMAC and MAC criterion: a) AutoMAC high-speed camera; b) AutoMAC accelerometers c) MAC high-speed camera/accelerometers.

A schematic representation of each used model is shown in Fig. 6, together with the location of the impact.

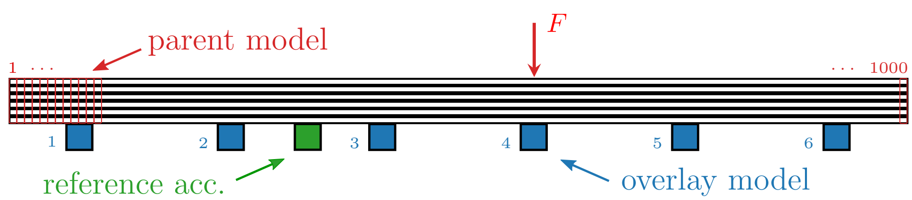

Figure 6: Schematic representation of the different models for the hybrid estimation of full-field FRFs.

4.3 Results

The final FRF of the hybrid model at the reference position is depicted in 3D in Fig. 7, together with the FRF from combined accelerometer/camera approach, identified FRF from the high-speed camera and the reference measurement. For all the configurations, the real and imaginary part of the FRFs are additionally presented in Fig. 8.

Below the 2-kHz range, where the noise on the identified displacements from the high-speed camera is not dominant, the overall shape of the reconstructed FRFs from the combined accelerometer/camera approach agrees well with reference measurement. Above 2 kHz the noise becomes dominant and the deviation in the displacement amplitude as well as an inconsistency in the overall shape of the FRF can be observed more clearly. In contrast, the proposed hybrid model accurately predicts the shape and the amplitude of both the real and the imaginary parts of the

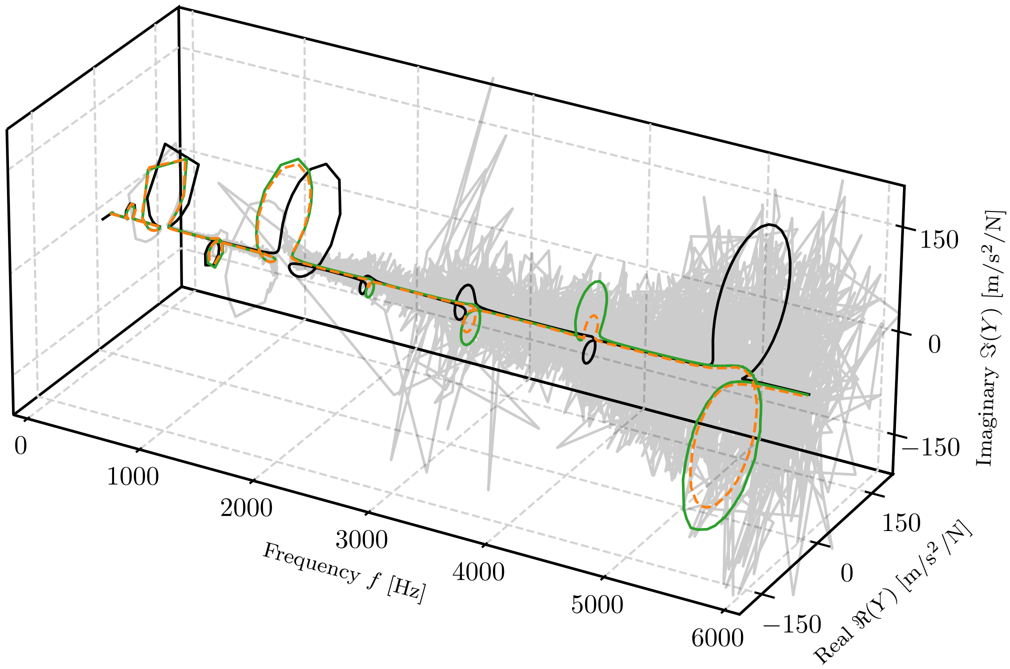

Figure 7: Comparison of different FRFs at the reference position displayed in 3D. Raw camera (——), combined accelerometer/camera (——), reference accelerometer (——), hybrid model (- - -)

reconstructed FRFs in the low- as well as in the high-frequency range. The inconsistent shape of the real and imaginary parts in the high-frequency range (combined accelerometer/camera identification) indicates the discrepancies in the overall phase of the FRFs. These deviations can be clearly seen from a Nyquist diagram in the region around 6th and 8th natural frequencies (Fig. 9). However, the alignment of the reconstructed FRFs from the hybrid model correlates well with the FRFs from the reference acceleration measurement. This indicates that the hybrid model correctly predicts the phase angle of the dynamic response.

Additionally, a coherence criterion [41] was used to objectively evaluate the performance and accuracy of the hybrid approach:

$$\chi = \mathrm{coh}(\mathrm{Y}, \mathrm{Y}_{\mathrm{ref}}) = \frac{(\mathrm{Y} + \mathrm{Y}_{\mathrm{ref}})(\mathrm{Y}^* + \mathrm{Y}^*_{\mathrm{ref}})}{2(\mathrm{Y}^*\,\mathrm{Y} + \mathrm{Y}^*_{\mathrm{ref}}\,\mathrm{Y}_{\mathrm{ref}})}, \tag{15}$$

where $\mathrm{Y}_{\mathrm{ref}}$ presents the reference FRF obtained from the accelerometer measurement.[4] In the lower-frequency range (for the first three natural frequencies), high coherence values of the FRFs can be observed, both for the combined accelerometer/camera and the hybrid approach. In the higher-frequency range, the coherence

[4]The coherence value $\chi = \mathrm{coh}(x, y)$ is equal to one if there is a perfect correlation between the two complex numbers ($x = y$) and the value is equal to zero if there is no correlation between the two ($x = -y$).

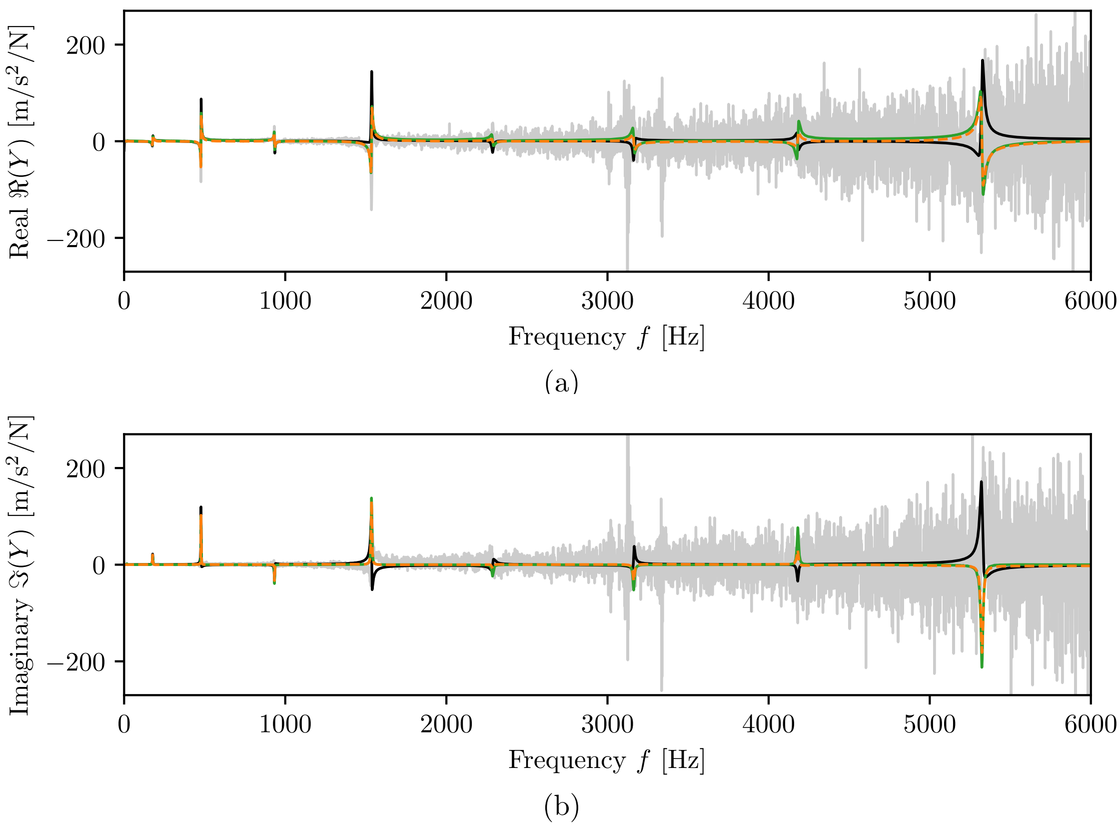

Figure 8: Comparison of different FRFs at the reference position; a) real part, b) imaginary part. Raw camera (——), combined accelerometer/camera (——), reference accelerometer (——), hybrid model (- - -).

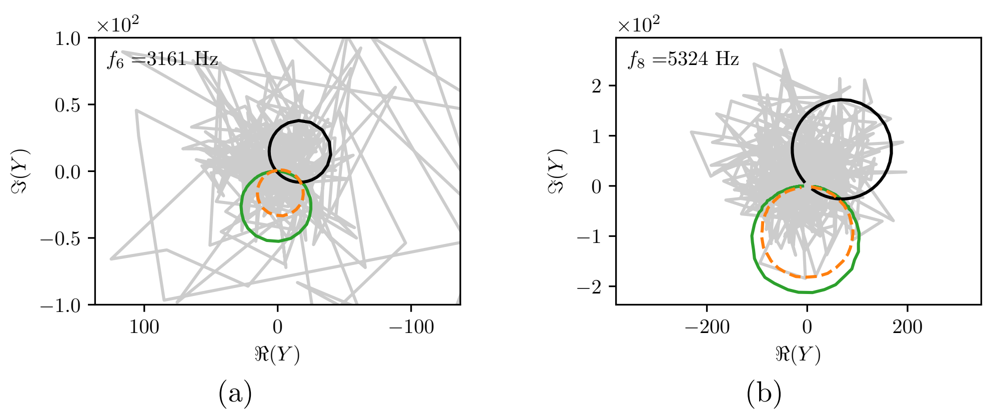

Figure 9: Comparison of different FRFs at the reference position on a Nyquist plot: a) 6th nat. frequency; b) 8th nat. frequency. Raw camera (——), combined accelerometer/camera (——), reference accelerometer (——), hybrid model (- - -).

values of the FRFs obtained using the combined accelerometer/camera approach gradually decrease; however, the hybrid approach retains the high coherence values of the FRFs also in this frequency region. The hybrid approach, in which two different experimental models are mixed using a dynamic substructuring approach, can evidently increase the reliability and consistency of the full-field FRFs estimated from the high-speed-camera data.

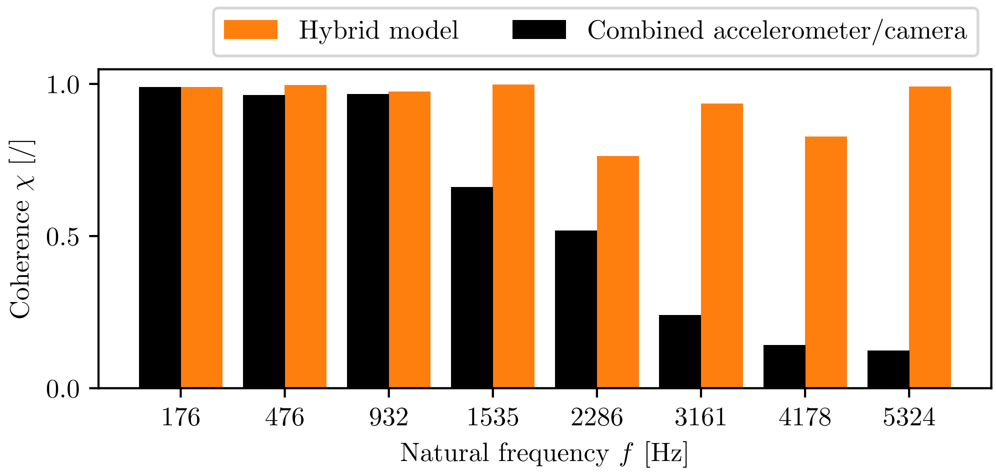

Figure 10: Comparison of mean coherence values around each natural frequency for both hybrid and combined accelerometer/camera FRFs evaluated with the reference measurement.

4.3.1. Size of the overlay model

The required numbers of DoFs used in the overlay model depends on the dynamic properties of the observed structure. Nevertheless, even an overlay model with a relatively small size of DoFs can be used to form a consistent hybrid model [30]. Therefore, the required size of the overlay model is case specific. The overlay model should be able to observe the relevant dynamic properties of the system (even one DoF may be sufficient in certain limit cases).

For the displayed experimental case the number of DoFs used in the overlay model can be reduced. In Fig. 11 a comparison of two different hybrid models is depicted. The first hybrid model is where all 6 DoFs measured with the accelerometers are included. The second hybrid model is formed from a reduced overlay model where only 2 DoFs are used (the locations used for both hybrid models are graphically depicted in Figure 11 legend). It can be observed that even with a reduced overlay model the inconsistencies in real and imaginary part of the FRFs in the high frequency range are resolved.

4.4 Discussion

The proposed methodology relies on the identified DoF of the high speed camera which are used as a parent model in SEMM (i.e. no numerical or analytical model is required for the expansion). Therefore, only the identified DoFs are available in the

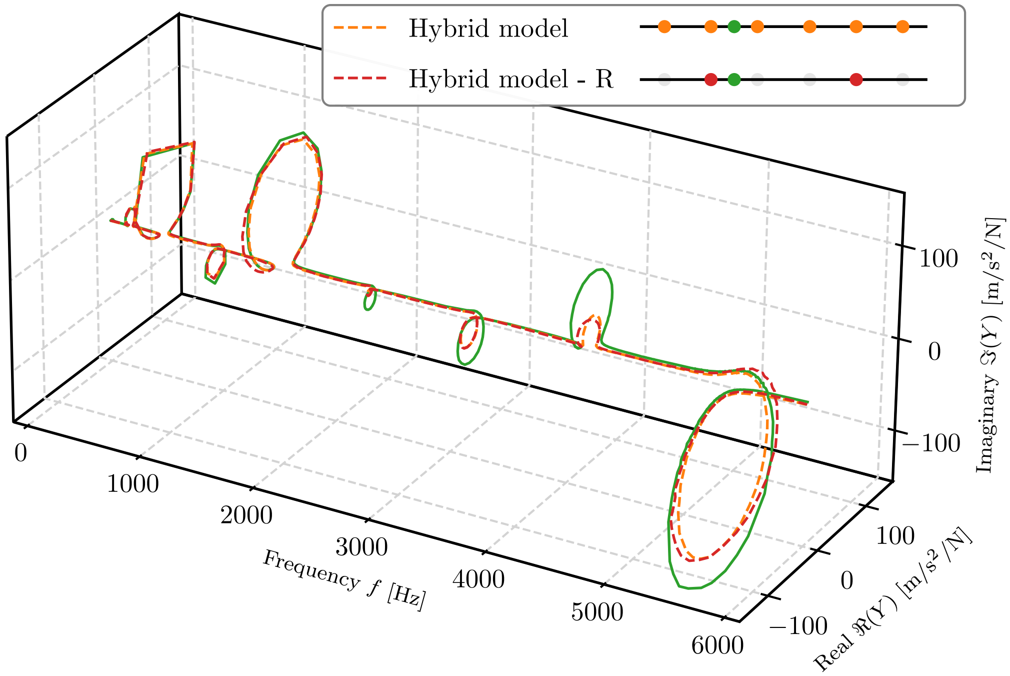

Figure 11: Comparison of different FRFs at the reference position displayed in 3D. Reference accelerometer (——), hybrid model (- - -), hybrid model - reduced (- - -).

full-field FRF estimation. If only a single-camera system is used, the out-of-plane motion cannot be identified from a single set-up. If a stereo pair is used, also the out-of-plane DoF can be identified [1]. In addition, if a large part of the structure is hidden from the camera field of view, those DoF cannot be identified. However, a multi-view system [42] or frequency domain triangulation [32] can be used to acquire spatial measurements that would otherwise not be available.

Furthermore, SEMM could also be used to expand the identified full-field FRFs on DoF that are outside the field of view. This can be achieved by using a numerical model or analytical as a parent model. A similar methodology was implemented in the modal domain with System Equivalent Reduction Expansion Process (SEREP) [43], where strain shape expansion was applied on optical measurements.

5 Conclusions

This research presents a hybrid approach to reconstructing full-field FRFs from high-speed-camera measurements using a dynamic substructuring approach. The displacements identified by the high-speed camera are very noisy due to the relatively small displacements caused by the vibrations, particularly in the high-frequency range. The novel approach presented in this paper proposes mixing two different experimental models in order to accurately estimate the full-field FRFs over the whole frequency range. Two experimental models are combined using the frequency-based substructuring to obtain a consistent hybrid model. The first model is obtained from the reconstructed full-field FRFs obtained from the combined accelerometer/camera identification and the second model is the accelerometer measurements, which are already used in the mode-shape identification. The mixing of the models yields the best combination of the two models. The dynamic properties are provided from an accurate FRF model (e.g., accelerometers) and the full-field DoF set is obtained from the high-speed camera measurements. Finally, it was shown that the hybrid approach can increase the reliability and consistency of the full-field FRFs. Consistent FRFs are obtained over a wide frequency range, even if the noise is predominant in the high-speed-camera data.

Acknowledgements

The authors acknowledge the partial financial support from the Slovenian Research Agency (research projects L2-1837 and N2-0144).

References

[1] M. N. Helfrick, C. Niezrecki, P. Avitabile, and T. Schmidt. 3D digital image correlation methods for full-field vibration measurement. *Mechanical Systems and Signal Processing*, 25:917–927, 2011.

[2] J. Baqersad, P. Poozesh, C. Niezrecki, and P. Avitabile. Photogrammetry and optical methods in structural dynamics – a review. *Mechanical Systems and Signal Processing*, 86:17–34, 2017.

[3] C. Schedlinski, J. Schell, E. Biegler, and J. Sauer. Application of optical measurement techniques for experimental modal analyses of lightweight structures. In *Proceedings of ISMA2016*, 2016.

[4] S. J. Rothberg, M. S. Allen, P. Castellini, D. Di Maio, J. J. J. Dirckx, D. J. Ewins, B. J. Halkon, P. Muyshondt, N. Paone, T. Ryan, H. Steger, E. P. Tomasini, S. Vanlanduit, and J. F. Vignola. An international review of laser doppler vibrometry: Making light work of vibration measurement. *Optics and Lasers in Engineering*, 99:11–22, 2017.

[5] D. A. Ehrhardt, M. S. Allen, S. Yang, and T. J. Beberniss. Full-field linear and nonlinear measurements using continuous-scan laser doppler vibrometry and high speed three-dimensional digital image correlation. *Mechanical Systems and Signal Processing*, 86:82–97, 2017.

[6] F. Trebuňa and M. Hagara. Experimental modal analysis performed by high-speed digital image correlation system. *Measurement*, 50:78–85, April 2014.

[7] L. Felipe-Sesé, Á. J. Molina-Viedma, E. López-Alba, and F. A. Díaz. FPDIC for low-cost 3d full-field experimental modal analysis in industrial components. *Mechanical Systems and Signal Processing*, 128:329–339, August 2019.

[8] J. Carr, J. Baqersad, C. Niezrecki, and P. Avitabile. Full-field dynamic strain on wind turbine blade using digital image correlation techniques and limited sets of measured data from photogrammetric targets. *Experimental Techniques*, 40(2):819–831, March 2016.

[9] T. Schmidt, J. Tyson, and K. Galanulis. Full-field dynamic displacement and strain measurement using advanced 3d image correlation photogrammetry: part 1. *Experimental Techniques*, 27(3):47–50, May 2003.

[10] V. Srivastava and J. Baqersad. An optical-based technique to obtain operating deflection shapes of structures with complex geometries. *Mechanical Systems and Signal Processing*, 128:69–81, August 2019.

[11] T. Liu, A. W. Burner, T. W. Jones, and D. A. Barrows. Photogrammetric techniques for aerospace applications. *Progress in Aerospace Sciences*, 54:1–58, October 2012.

[12] P. Poozesh, A. Sabato, Aral Sarrafi, C. Niezrecki, P. Avitabile, and R. Yarala. Multicamera measurement system to evaluate the dynamic response of utility-scale wind turbine blades. *Wind Energy*, March 2020.

[13] A. Khadka, B. Fick, A. Afshar, M. Tavakoli, and J. Baqersad. Non-contact vibration monitoring of rotating wind turbines using a semi-autonomous UAV. *Mechanical Systems and Signal Processing*, 138:106446, April 2020.

[14] W. H. Peters and W. F. Ranson. Digital Imaging Techniques In Experimental Stress Analysis. *Optical Engineering*, 21, 1982.

[15] B. Pan, K. Li, and W. Tong. Fast, Robust and Accurate Digital Image Correlation Calculation Without Redundant Computations. *Experimental Mechanics*, 53:1277–1289, 2013.

[16] J. Javh, J. Slavič, and M. Boltežar. The subpixel resolution of optical-flow-based modal analysis. *Mechanical Systems and Signal Processing*, 88:89–99, 2017.

[17] B. D. Lucas, T. Kanade, et al. An iterative image registration technique with an application to stereo vision. In *International Joint Conference on Artificial Intelligence*. Vancouver, British Columbia, 1981.

[18] D. J. Fleet and A. D. Jepson. Computation of component image velocity from local phase information. *International Journal of Computer Vision*, 5:77–104, 1990.

[19] A. Sarrafi, Z. Mao, C. Niezrecki, and P. Poozesh. Vibration-based damage detection in wind turbine blades using phase-based motion estimation and motion magnification. *Journal of Sound and Vibration*, 421:300–318, May 2018.

[20] T. J. Beberniss and D. A. Ehrhardt. High-speed 3d digital image correlation vibration measurement: Recent advancements and noted limitations. *Mechanical Systems and Signal Processing*, 86:35–48, 2017.

[21] P. Guillaume, L. Hermans, and H. Van der Auwerer. Maximum Likelihood Identification of Modal Parameters from Operational Data. *Proceedings of the 17th International Modal Analysis Conference*, 1999.

[22] H. Van Der Auweraer, W. Leurs, P. Mas, and L. Hermans. Modal parameter estimation from inconsistent data sets. In *Proceedings of SPIE - The International Society for Optical Engineering*, volume 4062, 2000.

[23] B. Peeters, H. Van der Auweraer, P. Guillaume, and J. Leuridan. The polymax frequency-domain method: a new standard for modal parameter estimation? *Shock and Vibration*, 11:395–409, 2004.

[24] J. Javh, J. Slavič, and M. Boltežar. High frequency modal identification on noisy high-speed camera data. *Mechanical Systems and Signal Processing*, 98:344–351, 2018.

[25] D. de Klerk, D. J. Rixen, and S. N. Voormeeren. General framework for dynamic substructuring: History, review and classification of techniques. *AIAA Journal*, 46:1169–1181, 2008.

[26] S. W. B. Klaassen, M. Van der Seijs, and D. de Klerk. System equivalent model mixing. *Mechanical Systems and Signal Processing*, 105:90–112, 2018.

[27] A. Drozg, G. Čepon, and M. Boltežar. Full-degrees-of-freedom frequency based substructuring. *Mechanical Systems and Signal Processing*, 98:570–579, 2018.

[28] J. E. Mottershead and M. I. Friswell. Model updating in structural dynamics: A survey. *Journal of Sound and Vibration*, 167(2):347–375, October 1993.

[29] D. de Klerk, D. J. Rixen, and J. de Jong. The Frequency Based Substructuring (FBS) Method reformulated according to the Dual Domain Decomposition Method. *in: Proceedings of the 24th International Modal Analysis Conference, A Conference on Structural Dynamics*, 2006.

[30] S. W. B. Klaassen and M. V. van der Seijs. Introducing SEMM: A Novel Method for Hybrid Modelling. *Conference Proceedings of the Society for Experimental Mechanics Series*, 4:117–125, 2018.

[31] Z. L. Kahn-Jetter and T. C. Chu. Three-dimensional displacement measurements using digital image correlation and photogrammic analysis. *Experimental Mechanics*, 30(1):10–16, 1990.

[32] D. Gorjup, J. Slavič, and M. Boltežar. Frequency domain triangulation for full-field 3d operating-deflection-shape identification. *Mechanical Systems and Signal Processing*, 133:106287, November 2019.

[33] B. Cauberghe. *Applied frequency-domain system identification in the field of experimental and operational modal analysis.* PhD thesis, Vrije Universiteit Brussel, 2004.

[34] R. J. Guyan. Reduction of stiffness and mass matrices. *AIAA Journal*, 3(2):380–380, February 1965.

[35] P. Avitabile. Model reduction and model expansion and their applications part 1 - theory. *Conference Proceedings of the Society for Experimental Mechanics Series*, 01 2005.

[36] J. C. O'Callahan, P. Avitabile, and R. Riemer. System equivalent reduction expansion process (SEREP). *Proceedings of the VII International Modal Analysis Conference (IMAC), Boston, MA*, 1:29–37, 1989.

[37] L. Thibault, A. Butland, and P. Avitabile. Variability improvement of key inaccurate node groups – VIKING. In *Topics in Modal Analysis II, Volume 6*, pages 603–624. Springer New York, 2012.

[38] B. Starc, G. Čepon, and M. Boltežar. The influence of washing machine-leg hardness on its dynamics response within component-mode synthesis techniques. *International Journal of Mechanical Sciences*, 127:23–30, July 2017.

[39] E. Pasma, W. B. S. Klaassen, M. Van der Seijs, and D. Lennström. Application of system equivalent model mixing (SEMM) to model the structural dynamic properties of a complex vehicle component using numerical and experimental data. In *Proceedings of ISMA2018*, 2018.

[40] J. W. R. Meggitt, A. T. Moorhouse, and A. S. Elliott. On the problem of describing the coupling interface between substructures: An experimental test for 'completeness'. In *Dynamics of Coupled Structures, Volume 4*, pages 171–182. Springer International Publishing, 2018.

[41] M. van der Seijs, D. van den Bosch, D. Rixen, and D. de Klerk. An improved methodology for the virtual point transformation of measured frequency response functions in dynamic substructuring. In *Proceedings of the 4th International Conference on Computational Methods in Structural Dynamics and Earthquake Engineering*. Institute of Structural Analysis and Antiseismic Research School of Civil Engineering National Technical University of Athens (NTUA) Greece, 2014.

[42] B. Pan. Digital image correlation for surface deformation measurement: historical developments, recent advances and future goals. *Measurement Science and Technology*, 29(8):082001, June 2018.

[43] K. Bharadwaj, A. Sheidaei, A. Afshar, and J. Baqersad. Full-field strain prediction using mode shapes measured with digital image correlation. *Measurement*, 139:326–333, June 2019.